ADVANCES IN ATMOSPHERIC SCIENCES, VOL. 38, SEPTEMBER 2021, 1566–1579

• **Original Paper** •

The Initial Errors in the Tropical Indian Ocean that Can Induce a Significant "Spring Predictability Barrier" for La Niña Events and Their Implication for Targeted Observations

Qian ZHOU[1], Wansuo DUAN[*2], Xu WANG[3], Xiang LI[1], and Ziqing ZU[1]

[1]*Key Laboratory of Marine Hazards Forecasting*, *National Marine Environmental Forecasting Center*, *Ministry of Natural Resources*, *Beijing* 100081, *China*

[2]*LASG*, *Institute of Atmospheric Physics*, *Chinese Academy of Sciences*, *Beijing* 100029, *China*

[3]*Ministry of Education Key Laboratory for Earth System Modeling*, *Department for Earth System Science*, *Tsinghua University*, *Beijing* 100084, *China*

(Received 15 December 2020; revised 12 March 2021; accepted 31 March 2021)

ABSTRACT

Initial errors in the tropical Indian Ocean (IO-related initial errors) that are most likely to yield the Spring Prediction Barrier (SPB) for La Niña forecasts are explored by using the CESM model. These initial errors can be classified into two types. Type-1 initial error consists of positive sea temperature errors in the western Indian Ocean and negative sea temperature errors in the eastern Indian Ocean, while the spatial structure of Type-2 initial error is nearly opposite. Both kinds of IO-related initial errors induce positive prediction errors of sea temperature in the Pacific Ocean, leading to under-prediction of La Niña events. Type-1 initial error in the tropical Indian Ocean mainly influences the SSTA in the tropical Pacific Ocean via atmospheric bridge, leading to the development of localized sea temperature errors in the eastern Pacific Ocean. However, for Type-2 initial error, its positive sea temperature errors in the eastern Indian Ocean can induce downwelling error and influence La Niña predictions through an oceanic channel called Indonesian Throughflow. Based on the location of largest SPB-related initial errors, the sensitive area in the tropical Indian Ocean for La Niña predictions is identified. Furthermore, sensitivity experiments show that applying targeted observations in this sensitive area is very useful in decreasing prediction errors of La Niña. Therefore, adopting a targeted observation strategy in the tropical Indian Ocean is a promising approach toward increasing ENSO prediction skill.

Key words: initial error, tropical Indian Ocean, La Niña prediction, sensitive area, targeted observation

Citation: Zhou, Q., W. S. Duan, X. Wang, X. Li, and Z. Q. Zu, 2021: The initial errors in the tropical Indian Ocean that can induce a significant "Spring Predictability Barrier" for La Niña events and their implication for targeted observations. *Adv. Atmos. Sci.*, **38**(9), 1566−1579, https://doi.org/10.1007/s00376-021-0427-1.

Article Highlights:

- Two types of IO-related initial errors that have the largest influence on La Niña predictions are explored.
- Type-1 and Type-2 IO-related initial errors can influence the SSTA associated with La Niña mainly via atmospheric bridge and ITF, respectively.
- The sensitive area in the Indian Ocean for La Niña predictions is mainly located in the tropical Eastern Indian Ocean.
- Adopting a targeted observation strategy in the sensitive area in the tropical Indian Ocean can significantly improve La Niña prediction skill.

1. Introduction

El Niño–Southern Oscillation (ENSO) is the most important air-sea coupling system in the tropical Pacific Ocean and can exhibit the largest influence on interannual variability in the world. The occurrences of ENSO events usually bring severe weather and climate disasters to many regions across the world (Barber and Chavez, 1983; Wang et al., 2000; Henderson et al., 2018; Yang et al., 2018). Therefore, it is very necessary to study ENSO theory and improve ENSO prediction skill (Kirtman et al., 2001; Zhu et al., 2013; Zhang et al., 2020a).

ENSO predictability is largely impacted by the air-sea

* Corresponding author: Wansuo DUAN
Email: duanws@lasg.iap.ac.cn

interaction process in the tropical Pacific Ocean (McPhaden, 2003). Great efforts are made to explore the predictors and optimal forcing of El Niño events in the tropical Pacific Ocean (Moore et al., 2006; Bunge and Clarke, 2014; Lopez and Kirtman, 2014; Duan and Hu, 2016). Recently, more and more studies have suggested that information from outside the tropical Pacific Ocean, like from the subtropical Pacific Ocean (Matei et al., 2008; Lu et al., 2017) and the Atlantic Ocean (Rodríguez-Fonseca et al., 2009; Ham et al., 2014), also plays a vital role in influencing ENSO predictions. Besides the sea temperatures in the Pacific Ocean, the oceanic state in the tropical Indian Ocean also influences the ENSO forecast in the Pacific Ocean (Behera and Yamagata, 2003; Luo et al., 2010). Lim and Hendon (2017) pointed out that strong negative Indian Ocean Dipole (IOD) events acted as a promoter of the weak La Niña during 2016. The ENSO simulation from Coupled General Circulation Model (CGCM) including both the tropical Pacific Ocean and the Indian Ocean tends to be more realistic than considering the tropical Pacific Ocean only (Yu et al., 2002). In statistical forecasting models, using Indian Ocean Dipole Mode Index (DMI) as a predictor can also significantly improve the ENSO forecasting skill (Izumo et al., 2010, 2014). The Indian Ocean Dipole can affect the strength of the Walker Circulation in autumn and lead to the development of ENSO events. Gear-like coupling between the Indian and Pacific oceans (GIP) is one of the atmospheric bridge theories developed to interpret the interactions between the air-sea interaction phenomena over the tropical Pacific and the Indian Ocean (Wu and Meng, 1998). A positive rotating GIP normally has an anticlockwise monsoon anomaly (westerly wind anomaly at the low-level and easterly wind anomaly at the upper-level) over the tropical Indian Ocean and a clockwise Walker Circulation anomaly (easterly wind anomaly at the low-level and westerly wind anomaly at the upper-level) over the tropical Pacific Ocean, while a negative GIP consists of a clockwise wind anomaly over the Indian Ocean and an anticlockwise Walker Circulation anomaly in the tropical Pacific Ocean. Meng and Wu (2000) have also verified that the ENSO events in the tropical Pacific Ocean can be triggered via GIP since the zonal wind anomaly in the tropical Indian Ocean can influence the air-sea coupling system in the Pacific Ocean. Along with the atmospheric bridge over the tropical oceans, the Indonesian Throughflow (ITF), the only oceanic channel connecting the tropical Indian Ocean and the tropical Pacific Ocean, also stands out as one of the dynamical mechanisms behind the IOD forcing influencing the ENSO-related SSTA (Yuan et al., 2011, 2013; Zhou et al., 2015).

From the perspective of error growth, the influence of sea temperature in the tropical Indian Ocean on ENSO predictions cannot be ignored. Two types of initial errors of sea temperature in the tropical Indian Ocean have been explored and found to be most likely to yield the Spring Prediction Barrier (SPB) of El Niño prediction (Zhou et al., 2019), suggesting the possibility that applying targeted observation strategies in the locations of the initial errors can further improve El Niño prediction skill (Zhou et al., 2020). Investigations of error evolution mechanisms show that for Type-1 initial error with positive IOD-like structure, the ITF plays a dominant role in influencing SSTA in the tropical Pacific Ocean, but for Type-2 initial error, the atmospheric bridge works as the main way to impact El Niño prediction. Each study mentioned above focused on the influences of IO-related initial errors on the predictability of El Niño events. However, as the negative phase of ENSO, La Niña events can also modulate the East Asian winter and summer monsoons (Huang et al., 2004; Xue et al., 2015), modulate the Mei-yu Rainfall over the Yangtze River Valley (Wang et al., 2012), and lead to severe wintertime droughts in northern China (Gao and Yang, 2009). Besides, the influences of La Niña events are worldwide. La Niña events can also influence sea temperature in the Atlantic Ocean (Wu et al., 2020) and snow accumulation in the Andes (Cortés and Margulis, 2017), leading to climatic anomalies in Europe (Ding et al., 2017). So, it is urgent to study the predictability of La Niña events and improve La Niña prediction skill. Given the influences of the initial state of the tropical Indian Ocean on the predictability of El Niño events, it is natural to ask: Will the initial errors of sea temperature in the tropical Indian Ocean influence La Niña predictability? Do the initial errors that are most likely to induce the SPB for La Niña and El Niño predictions share similar spatial structures? What is the mechanism behind the error evolutions? What is the implication of the targeted observation strategy for La Niña forecasts? All of these questions are addressed in this study.

In this paper, section 2 gives a brief description of the model and data. The experimental design is shown in section 3. The initial errors that are most likely to induce the SPB during La Niña prediction are investigated in section 4. The characteristics of the error evolutions and their dynamical mechanisms are analyzed in detail in section 5. In section 6, the implications of applying targeted observations in the tropical Indian Ocean are studied. The summary and discussion are presented in section 7.

2. Model and data

The Community Earth System Model (CESM), a coupled model designed by the National Center for Atmospheric Research (NCAR), is used in this study. The CESM has many model components, such as atmosphere, land, ocean, and ice, with a flux coupler to link them (Hurrell et al., 2013). The CESM's atmospheric component, CAM4, has a horizontal resolution of 0.9° latitude and 1.25° longitude, while the resolution of the oceanic component, POP, is $1° \times 1°$ in the off-equatorial area and is enhanced to 1/3° latitude by 1° longitude in the tropics. This coupled model is integrated for 150 years forced by values of tracer gases, aerosols, insolation, and land cover from the year 2000. In this study, we only take the simulations from year 51 to year 150 (a total of 100 model years).

As a coupled model, the CESM's simulations of the sea temperature states (i.e., the climatology state and standard deviations) in the tropical Indian Ocean and the Pacific Ocean are in good agreement with the observations. ENSO dominates as the leading mode in the tropical Pacific Ocean, explaining nearly 51% of the total variances of the SST during the winter. The power spectrum of the Niño-3 index from the simulation shows a period of three to six years. Six typical La Niña events simulated by this model are shown in Fig. 1. These typical La Niña events which start cooling in Jan(0), usually reach their peak in Oct(0) and decay afterwards. Finally, these La Niña events change to the normal state in May(1). Here, "0" and "1" represent the La Niña year and the following year, respectively. This seasonal feature indicates that the CESM provides reasonable simulation of La Niña events' phase-locking feature. In the Indian Ocean, the dipole mode (i.e., positive sea temperature anomalies in the tropical western Indian Ocean and negative anomalies in the tropical eastern Indian Ocean) works as the leading mode and can explain 64% of the total variance.

The atmospheric bridge and the ITF are suggested as the most important ways for initial errors in the tropical Indian Ocean to impact the SSTA predictions in the tropical Pacific Ocean. So, the CESM's ability to simulate both the atmospheric bridge (GIP) and the ITF is investigated. In the climatological simulation, the rising branch of the atmospheric bridge is located over the western Pacific Ocean and the eastern Indian Ocean, where SSTs are warm; meanwhile, two sinking branches appear in the eastern Pacific Ocean and the tropical western Indian Ocean. Regarding the ITF, the volume transport along the IX01 line is commonly used to present the ITF. The IX01 XBT (expendable bathythermograph) line, which is part of XBT network of the Indian Ocean Observing System (IndOOS) (Hermes et al., 2019), almost crosses the Fremantle-Sunda Straits, which is a connection between the tropical Pacific Oceans and the Indian Ocean. On average, the ITF calculated from the CESM simulations is 10.7 Sv, and it usually peaks in the summer and decays in the winter, showing a seasonally dependent feature. These features simulated by the CESM are very consistent with the ITF observations (Gordon, 2005; Tillinger and Gordon, 2009).

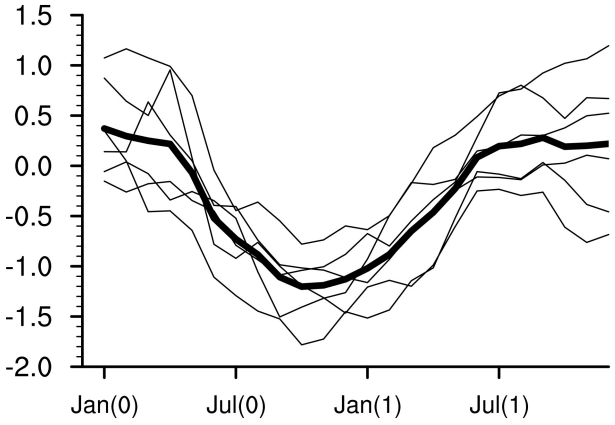

Fig. 1. Niño-3 index (units: °C) of six La Niña events from CESM1.0.3. The thin lines represent the six La Niña events and the thick line is the mean of the six events (here, "0" and "1" signify the La Niña year and the next year, respectively).

Besides the CESM's good performance on the simulations mentioned above, it can also simulate the role of the atmospheric bridge and the ITF in the IOD forcing that influences the SSTA in the tropical Pacific Ocean. Following the example of Yuan et al. (2013), analysis of the lag correlations between the IOD index with the SSTA in the tropical oceans is also carried out, and just like FGOALS-g2 (Xu et al., 2013), the CESM can simulate the ITF's role in IOD forcing influencing the SSTA associated with the ENSO, but the atmospheric bridge's role is overestimated when compared with the observations. The ITF's contributions are also further examined with sensitivity experiments carried out with the CESM (Zhou et al., 2015).

In short, the CESM can be used to study the influence of the initial errors in the tropical Indian Ocean on the predictability of La Niña.

3. Experimental design

Since the CESM can capture the essential features of La Niña events and the relevant interactions between the tropical Pacific Ocean and the Indian Ocean, it is reasonable to regard these model-simulated events from the CESM as "reference state" of the La Niña events. These La Niña events, as shown in Fig. 1, are then predicted for 12 months with sea temperature perturbations added only in the tropical Indian Ocean. These kinds of initial errors are marked as IO-related initial errors in this study. The differences between the predictions from the sensitivity experiments and the reference state (i.e., the "prediction errors") are induced only by these IO-related initial errors. This strategy is now widely used in the study of predictability from the perspective of error growth (Feng et al., 2014; Duan and Hu, 2016). Six La Niña years are chosen from the 100-year integration, as mentioned in section 2. Due to the huge computational cost of the sensitivity experiments, only sensitivity experiments starting from Jan(0) are completed. Since these predictions bestride the growing phase of La Niña, we are able to focus on the onsets of the La Niña events at the end of the prediction.

A number of sensitivity experiments are then carried out for the selected La Niña events in an attempt to explore the IO-related initial errors that are most likely to yield the SPB. Here, IO-related initial errors are obtained by the following steps: First, for each typical La Niña event simulated from the coupled model, the differences between the sea temperatures in the tropical Indian Ocean (40°–130°E, 10°S–10°N; 0–400 m, ranging from the 1st to 30th level in the ocean model) of the start month and every other month during the four years before the start month are obtained as the initial errors. Thus, for each La Niña event, 24 initial perturbations can be chosen. Taking simulation 0061-01 from the model as an example, the 24 initial errors are 0057-02,

0057-04, 0057-06, …, 0060-10, and 0060-12. These initial errors are marked as T', and their norms can be calculated according to $\| T' \| = \sqrt{\sum_{i,j,k} T'^2_{i,j,k}}$, where $T'_{i,j,k}$ is the values of T' at the grid point (i, j, k) in the tropical Indian Ocean, with i, j, k referring to the longitude, latitude, and vertical grid points, respectively. T' is then scaled to conditional initial error T'_0, following $T'_0 = (T'/\| T' \|)\delta$, where $T'_0 = \{T'_{0i,j,k}\}$, and δ is the climatological variation of sea temperature in the tropical Indian Ocean. These 24 conditional IO-related initial errors are then added at the start month, Jan(0), of the La Niña events and integrated for 12 months. Thus, for each La Niña event, we can get 24 predictions, and with 6 La Niña events, 144 predictions are obtained in total. Based on these predictions from the sensitivity experiments, prediction errors are calculated as the differences between the "reference state" La Niña event (the chosen La Niña event without any perturbation) and the predictions. Therefore, all prediction errors are only induced by the IO-related initial errors.

4. Two types of IO-related initial errors that can induce the SPB for La Niña predictions

In order to explore the initial errors that can induce a notable SPB for La Niña forecasts, a large number of sensitivity experiments are carried out with conditional initial errors of sea temperature superimposed only in the tropical Indian Ocean. Based on these 144 La Niña predictions, prediction errors can be measured according to $\lambda(t) = \| T^{\mathrm{p}}(t) - T^{\mathrm{r}}(t) \| = \sqrt{\sum_{i,j} [T^{\mathrm{p}}_{i,j}(t) - T^{\mathrm{r}}_{i,j}(t)]^2}$, where grid points (i, j) are from the Niño-3 region, with i and j referring to the longitude and latitude grid points, respectively, and T^{p} and T^{r} represent the SST of the predictions from sensitivity experiments and reference La Niña events, respectively. Parameter γ is defined as $\gamma = [\lambda(t_2) - \lambda(t_1)] / [t_2 - t_1]$ to evaluate the season-dependent growth of La Niña prediction errors, where $(t_2 - t_1)$ measures the time interval of a season, and $\lambda(t_2)$ and $\lambda(t_1)$ are the prediction errors at the final and start time of one season, respectively. Positive γ means the prediction errors grow during the season, and the lager the absolute value of the γ, the faster the error grows. In the present study, if the prediction errors of particular La Niña events grow quickly during the season of spring and the beginning of summer and remain large at the final time of the predictions, we conclude that an SPB occurs. Among the 144 IO-related initial errors, 45 of them are likely to induce a SPB during the La Niña predictions. For simplicity, we mark them as SPB-related initial errors.

In order to have a deeper understanding of the common features of the SPB-related initial errors, the evolution of the averaged prediction errors induced by both SPB-

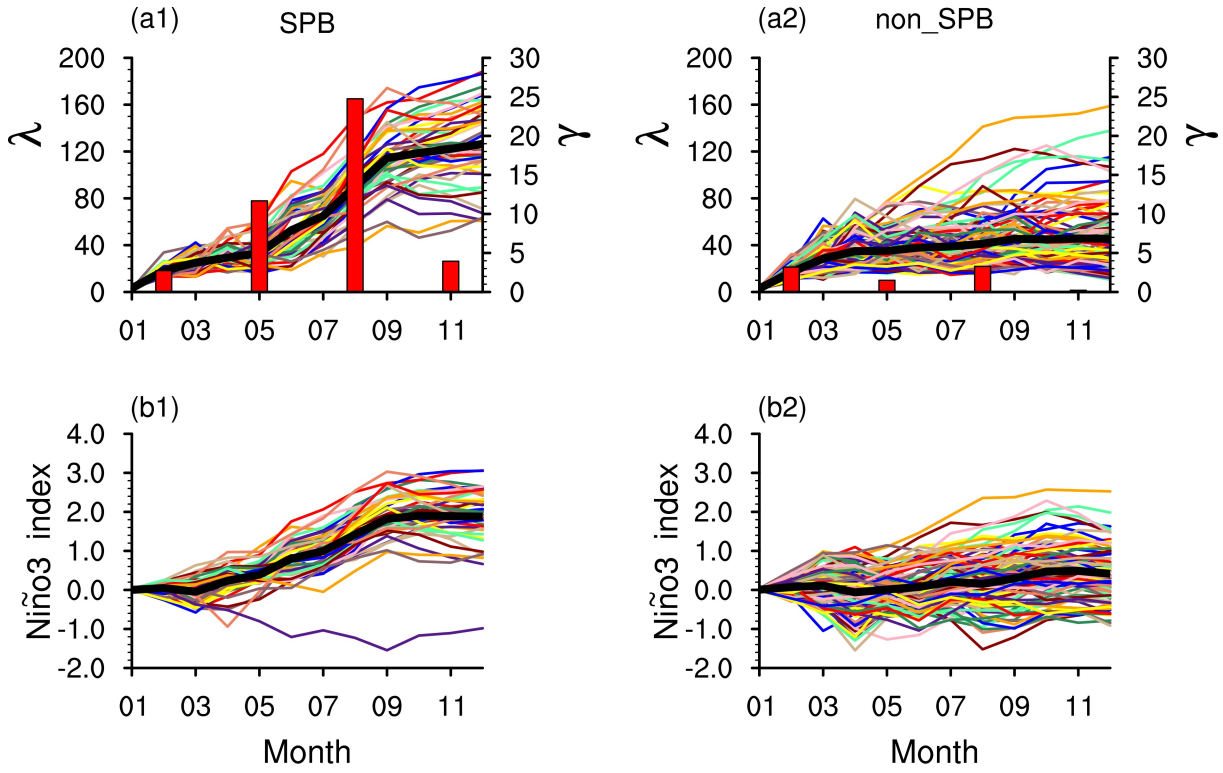

Fig. 2. (a1) The prediction errors (λ) caused by each SPB-related conditional initial error (colored curves) for the six La Niña events with the start month Jan (0) (the average is in bold black), where the average of the seasonal growth rates of prediction errors (γ) are also plotted in histograms; (a2) same as (a1), but for non_SPB-related conditional initial errors; (b1) and (b2) show the corresponding Niño-3 index errors (units: °C, colored curves) when compared with the control run and their averaged mean (bold black) for SPB-related and non_SPB-related conditional initial errors, respectively.

related and non_SPB-related initial errors are shown (the thick black line in Figs. 2a1 and 2b1). For SPB-related initial errors, the prediction errors increase rapidly during May(0) to Sep(0), eventually reaching very large values, indicating that April–May–June (AMJ) and July–August–September (JAS) are the seasons with quickest error increases during the forecasts. For non_SPB-related initial errors, the growth rates of the prediction errors during these seasons are quite small. Additionally, most of the predicted Niño-3 index errors induced by the SPB-related initial errors are positive and keep growing during the predictions, as seen in Fig. 2b1. These SPB-related initial errors tend to lead to La Niña events being underpredicted in terms of their magnitudes, and sometimes they even result in a forecast missing a La Niña event entirely.

Cluster analysis is applied to diagnose the common spatial features of the SPB-related initial errors obtained above, and two types of SPB-related initial errors are found, as shown in Fig 3. Among all 45 SPB-related initial errors, 18 are Type-1 initial errors (Fig. 3a1). We can see that Type-1 initial errors have a positive IOD-like spatial structure with positive sea temperature errors in the tropical western Indian Ocean and negative values in the east; while for the Type-2 initial errors, as shown in Fig. 3a2, the structure is almost opposite to that of the Type-1 initial errors (i.e., with negative errors in the western basin and positive errors in the east). These dipole-like features not only occur on the surface of the Indian Ocean, but also prevail in the subsurface regions (as shown in Figs. 3b1 and b2). The sea temperature errors in the subsurface can also modulate the influence on the sea surface temperature by vertical mixing and entrainment processes (Zhang and Zebiak, 2002; Zhu et al., 2020).

5. Mechanisms of the error evolution

From the sensitivity experiments concerning only IO-related initial errors, two types of initial errors that are most likely to yield the SPB are obtained, and the common features of their spatial structures are explored. But how will these initial errors develop and impact the SST predictions in the Pacific Ocean? In order to answer this question, the error evolutions and dynamical mechanisms behind them are studied in depth in this section.

The error evolutions of sea temperature Type-1 initial errors along the tropical oceans are composited in Fig. 4. When Type-1 initial errors are superimposed in the tropical Indian Ocean, the sea temperature errors exhibit a positive IOD-like pattern, and the magnitudes of the sea temperature errors are increased. In the tropical Pacific Ocean, the positive errors of sea temperature first appear in the eastern Pacific Ocean at the start month and continue growing afterwards. At the end of the predictions, the prediction errors in the tropical Indian Ocean and the tropical Pacific Ocean are positive IOD-like and El Niño-like, respectively.

For SPB-related Type-2 initial error, the composited error evolutions are displayed in Fig. 5. Unlike the evolution of Type-1 initial error, when Type-2 initial error is added in the tropical Indian Ocean, negative IOD-like sea temperature error patterns do not stay there through the end of the prediction. In fact, the positive errors in the eastern Indian Ocean diminish and turn to negative values during Apr(0), while negative errors in the western Indian Ocean convert to positive errors. This positive IOD-like pattern dominates in the tropical Indian Ocean in the end. Meanwhile in the tropical Pacific Ocean, positive sea temperature errors first show in the western Pacific Ocean. These positive

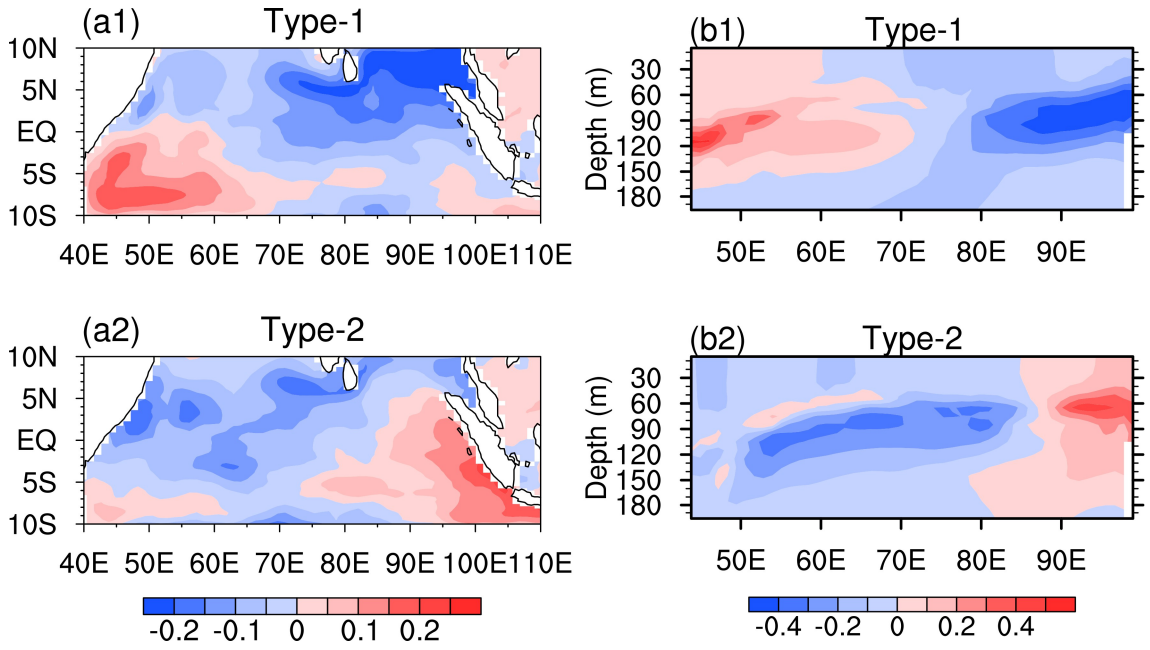

Fig. 3. The SST and the vertical sea temperature (averaged by meridian 5°N to 5°S) components of the Type-1 (a1 and b1) and Type-2 (a2 and b2) SPB-related initial errors for Jan (0).

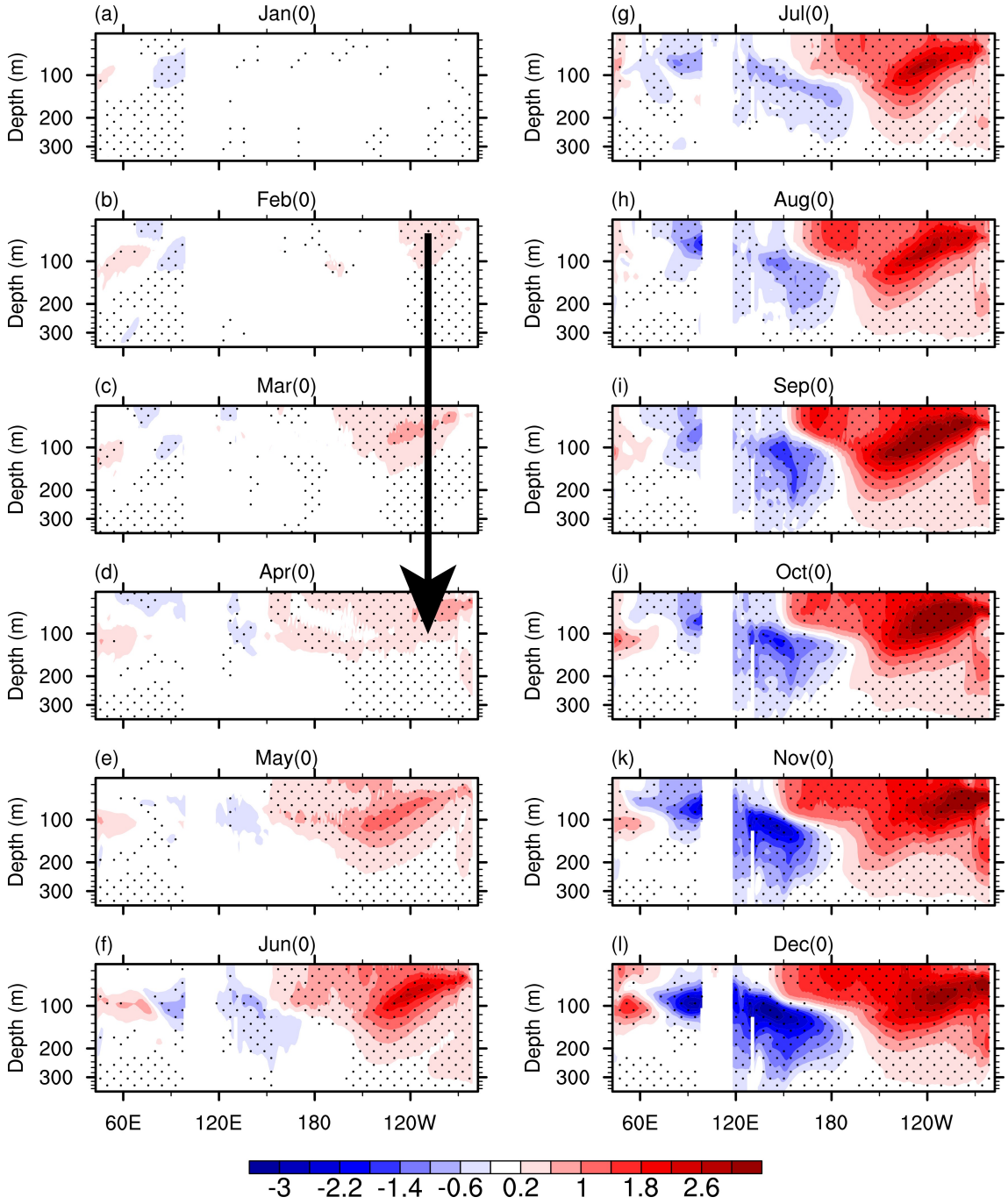

Fig. 4. The composite monthly sea temperature component (averaged meridional over 5°N to 5°S) for the evolutions of Type-1 initial error with the start month Jan(0) (the regions covered by dots indicates those of statistical significance (>95%). The evolution of sea temperature errors is highlighted as black arrow.

errors keep growing and propagate to the east Pacific Ocean, resulting in an El Niño-like error state in the end.

To sum up, in the tropical Indian Ocean, when SPB-related Type-1 initial error is added in the tropical Indian Ocean, the errors tend to keep growing with this kind of spatial structure, just like a positive IOD event experiencing a growing phase evolution; while for SPB-related Type-2 initial errors with a negative IOD-like mode, the prediction errors tend to decay and ultimately change to a positive IOD-like state. In the tropical Pacific Ocean, the sea temperature errors induced by the SPB-related Type-1 initial error experience localized developments in the eastern Pacific Ocean. Meanwhile, the prediction errors of sea temperature induced by Type-2 initial error usually first appear in the western Pacific Ocean and then propagate to the east.

It is clear that both kinds of SPB-related initial errors experience quite different evolutions in the two oceans. Why are they different and what are the dynamic mechan-

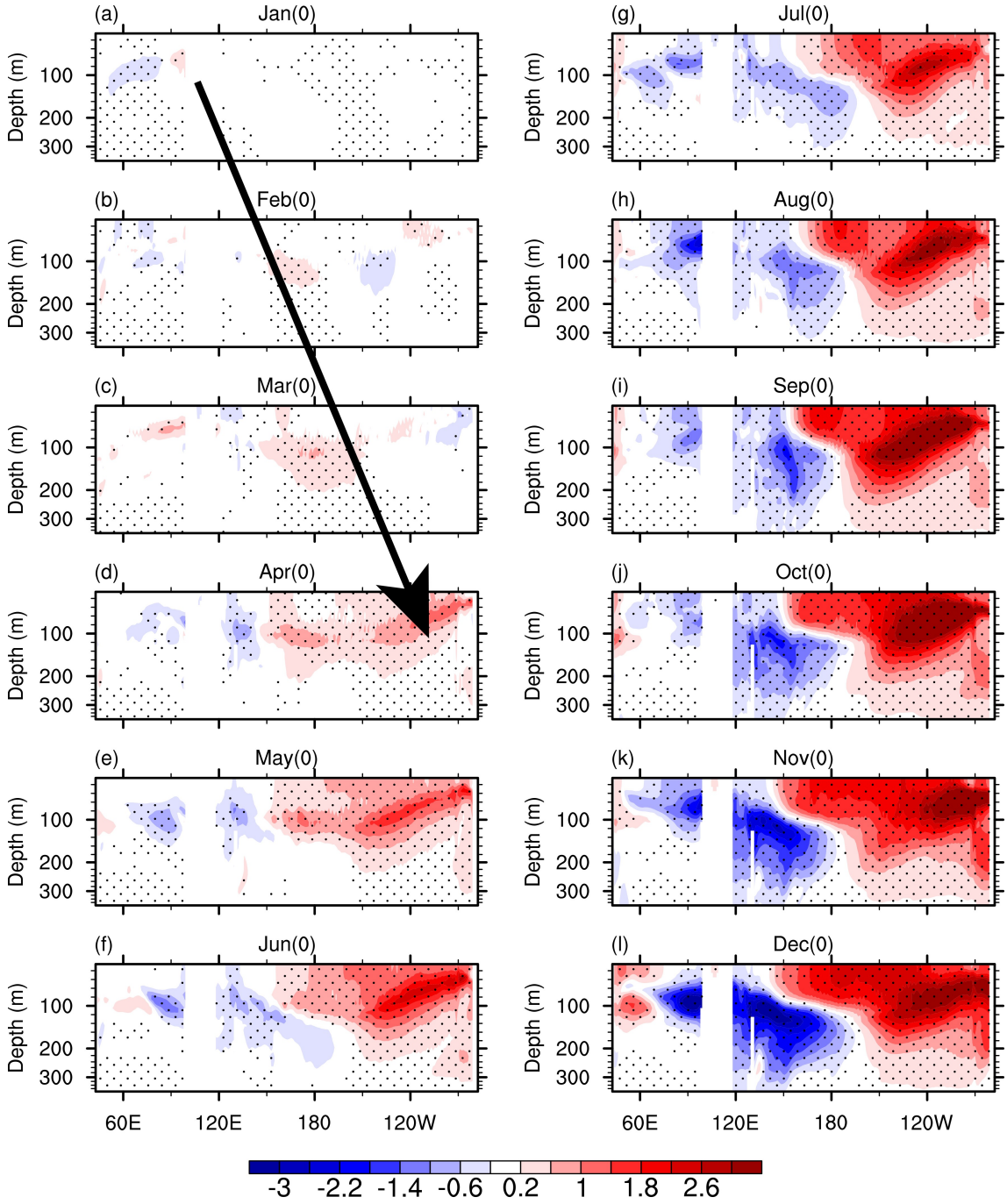

Fig. 5. As in Fig. 4, but for Type-2 initial error.

isms behind the error evolutions? Zhou et al. (2019) suggested that during El Niño predictions, either the ITF or the atmospheric bridge plays a vital role in IO-related initial errors influencing the SST predictions in the tropical Pacific Ocean. We cannot help wondering: Do these dynamical mechanisms still work in the La Niña predictions? Which role do they play in each kind of error evolutions? In order to make these clear, the roles of both the ITF and the atmospheric bridge (GIP) are studied.

First, we look into the role of the ITF. The averaged volume transport of the ITF anomalies calculated along the IX01 line for SPB-related Type-1 and Type-2 initial errors are −0.13 Sv and −0.50 Sv, respectively. Zhou et al. (2015) performed sensitivity experiments with the atmospheric bridge shut down, resulting in ITF anomalies induced by positive and negative IOD forcing of 6.18 Sv (positive) and −6.21 Sv (negative), respectively. It is clearly shown that the ITF anomalies induced by both Type-2 initial error in this study and that from negative IOD forcing are both negative, implying that the ITF may play a leading role in the evolution of Type-2 initial error. Since the ITF volume is defined as the amount of warm water transported from the

warm pool area in the western Pacific Ocean to the Indian Ocean, negative ITF error indicates that less warm water is transported from the western Pacific Ocean to the Indian Ocean, or anomalously warm water in the tropical eastern Indian Ocean penetrates into the western Pacific Ocean (Zhou et al., 2015), which may also be the dynamical mechanism of Type-2 initial error influencing the SST prediction in the Pacific Ocean.

In order to have a deeper understanding of the dynamical mechanisms, composited error evolutions of Type-2 initial error are plotted and shown in Fig. 6. It is clearly seen that positive sea surface height errors are induced by the positive sea temperature errors in the tropical eastern Indian Ocean, leading to local downwelling anomalies there. These downwelling anomalies further penetrate into the western Pacific Ocean, resulting in positive sea temperature errors. And, these positive errors of sea temperature keep traveling to the equatorial eastern Pacific Ocean, preserving an El Niño-like error pattern at the end of the prediction. So, the ITF's role in Type-2 initial errors influencing the SSTA predictions associated with La Niña is clear. But how about the role of the atmospheric bridge? Actually, according to the GIP theory, which is one of the popular atmospheric bridge theories, the positive errors in the eastern Indian Ocean tend to induce updraft errors over the Indian Ocean and downdraft errors over the Pacific Ocean, leading to negative SSTA prediction errors in the tropic Pacific Ocean. Meanwhile, positive SSTA prediction errors are the main errors during the whole prediction. So, it is the ITF, rather than the atmospheric bridge, that plays the leading role in Type-2 initial error influencing the La Niña predictions.

When it comes to the SPB-related Type-1 initial error, the induced ITF errors are also negative, which is of the opposite sign to the ITF anomalies induced by the negative IOD forcing when the atmospheric bridge was shut down (Zhou et al., 2015). According to Zhou et al. (2015), when positive IOD-like errors influence the SST predictions in the tropical Pacific Ocean through the ITF, the negative SST errors usually dominate in the tropical Pacific Ocean throughout the predictions, rather than inducing positive errors there. Thus, it is very unlikely for the ITF to play the chief role in IO-related initial errors influencing SSTA prediction in the Pacific Ocean since we have positive prediction errors of sea temperature in the Pacific Ocean during the La Niña forecasts. So, we must study the role of the atmospheric bridge. Evolutions of wind errors induced by the Type-1 initial errors are plotted in Fig. 7. It is shown that during Jan(0), when positive IOD-like errors of sea temperature are superimposed in the tropical Indian Ocean, downdraft errors appear both in the western Pacific Ocean and the eastern Indian Ocean. According to the GIP theory, these downdraft errors can lead to updraft errors in the central and eastern Pacific Ocean during Jan(0) and Feb(0). Those downdraft errors further induce positive errors of sea temperature in the eastern Pacific Ocean, resulting in many La Niña events being missed by forecasts. Therefore, SPB-related Type-1 initial errors in the Indian Ocean usually influence the sea temperature in the tropical Pacific Ocean mainly by virtue of the GIP.

To sum up, Type-1 and Type-2 SPB-related initial errors in the tropical Indian Ocean mainly influence the sea temperature predictions in the Pacific Ocean via GIP and the ITF, respectively.

6. Implications for targeted observations

During ENSO forecasts, data assimilation in coupled models is quite important (Gao et al., 2016; Zhang et al., 2020b), and a targeted observation strategy can provide additional valuable observations for the assimilation. To improve a forecast at time t_1 (verification time) in an area of concern (verification area), additional observations are

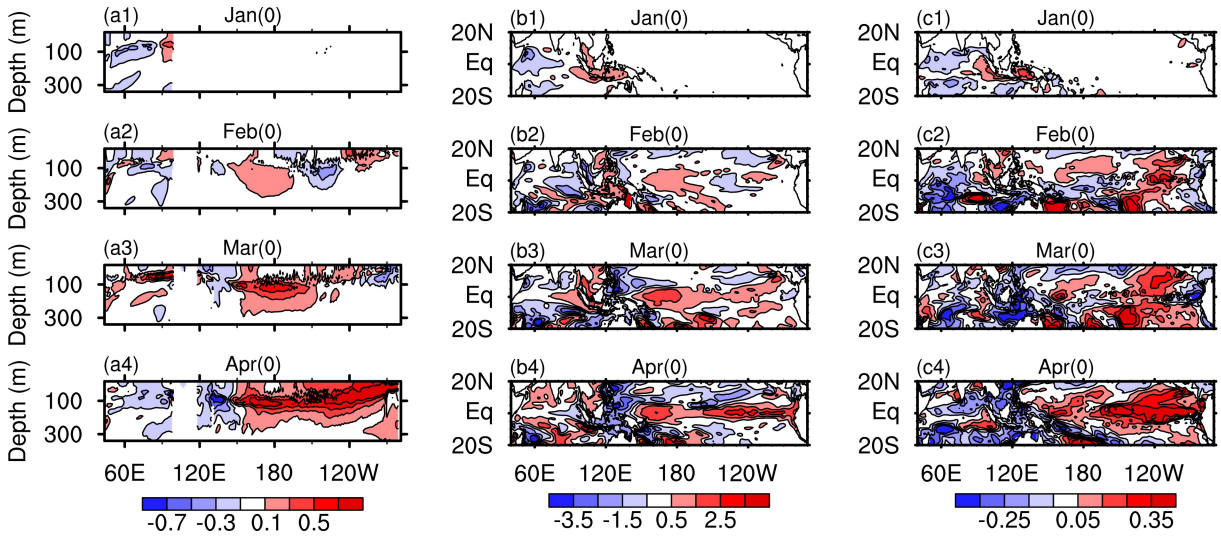

Fig. 6. Composited evolution of Type-2 initial error from Jan(0) to Apr(0) with the components of (a) the vertical sea temperature errors in tropical Indian Ocean and the Pacific Ocean over the equator, (b) the SSH errors, and (c) the SST errors.

deployed at a future time t_2 (target time; $t_2 < t_1$) in some key areas (sensitive area) where additional observations are expected to have a considerable contribution to the forecast in the verification area (Snyder, 1996; Mu, 2013; Mu et al., 2015). One challenge is the determination of the sensitive area. Normally, the locations of SPB-related initial errors with large values can be assumed as the sensitive areas for targeted observations (Mu et al., 2014; Duan and Hu, 2016). So, the large value area of SPB-related initial errors in the Indian Ocean may also be the sensitive area for La Niña predictions. In this study, the sensitive area is identified where the SPB-related initial errors are larger than 0.2°C. As shown in Fig. 8, the large values mainly exist in the subsurface of the eastern Indian Ocean, suggesting the possibility of this area being the sensitive area for La Niña predictions. Will the prediction skill be improved with targeted observations applied there? To answer this question, a number of sensitivity experiments are carried out. In sensitivity experiments with targeted observations applied inside the sensitive area, which are marked as Sensi-1, we simply wipe out the initial errors in the sensitive area and set the initial errors to zero. For sensitivity experiments with targeted observations applied outside the sensitive area, which are signified as Sensi-2, initial errors outside the sensitive area are erased. Here, predictions with the original initial errors superimposed (i.e., with no targeted observation strategy applied) are regarded as the control run.

The results of the targeted observations sensitivity experiments are shown in Table 1. The bulk of non-sensitive area in the tropical Indian Ocean is about 2.22×10^7 km^3, which is four times larger than the sensitive area. Although the area is much larger, adopting the targeted observation strategy in the non-sensitive area provides little help toward achieving better La Niña predictions. Surprisingly, the prediction skill is reduced (–0.14%) in general. From Sensi-1, where targeted observation strategies are applied inside the sensitive area, La Niña prediction skill can be improved by 20.59%. The averaged benefit is defined following Zhou et al. (2020) (i.e., β= improvement of La Niña prediction skill / volume of the area with targeted observations applied). Here, β measures the effectiveness of adopting targeted observation strategies since it can represent the prediction skill improvement per km^3 for a certain area. In this study, the effectiveness β from both Sensi-1 and Sensi-2 are calculated. β of Sensi-1 is very large, reaching up to 399.90; β of Sensi-2 is –0.06 on average. Although the sensitive area occupies a very small area of the tropical Indian Ocean, it is very effective to adopt targeted observation strategy there to reduce the prediction errors of the La Niña forecasts.

Prediction errors of sea temperature from the control run, Sensi-1, and Sensi-2 are shown in Fig. 9. In the control run, without any targeted observations applied, positive sea temperature errors dominate as the main feature at the end of the forecasts, as shown in Fig. 9a. In Fig. 9b, where tar-

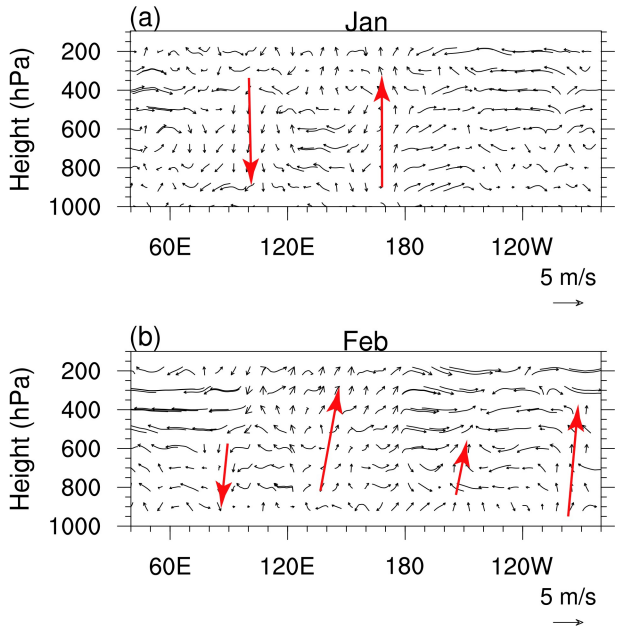

Fig. 7. Wind error evolutions induced by the Type-1 initial error during Jan (0) and Feb (0) (averaged by meridian 5°N to 5°S). The updraft and downdraft branches are highlighted as red arrows.

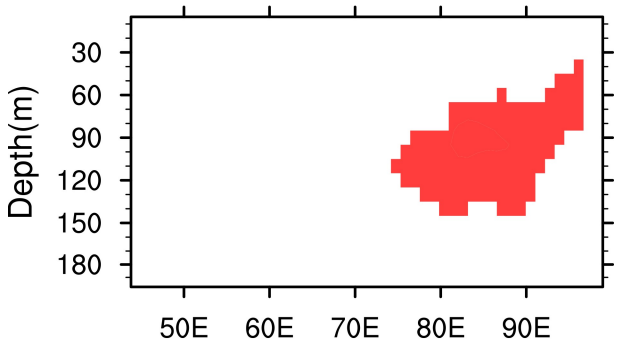

Fig. 8. The sensitive area (shaded in red) of targeted observations in the tropical Indian Ocean for the La Niña predictions.

Table 1. The averaged prediction errors and the averaged benefits of the targeted observation strategy conducted inside/outside the sensitive area for La Niña predictions.

	Sensi-1	Sensi-2
Prediction errors for Exp-ref (Err_0)	101.32	101.32
Predictions errors with targeted observations (Err)	80.46	101.46
The improvement for El Niño events ($1 - Err/Err_0$)	20.59%	–0.14%
The bulk of sensitive area (10^7 km^3)	0.52	2.22
Averaged benefit for the targeted observation β (10^{-7} km^{-3})	399.90	–0.06

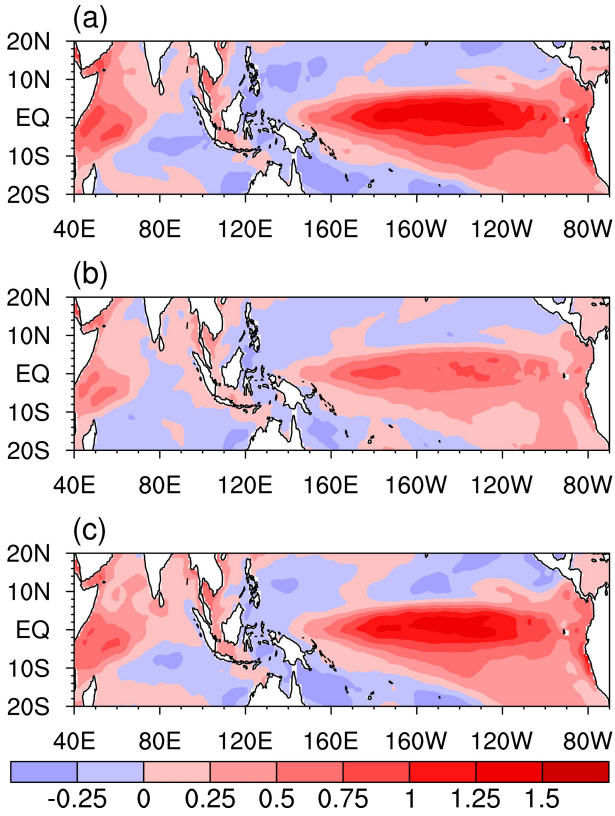

Fig. 9. Prediction errors in Dec(0) in the tropical oceans for La Niña predictions starting from Jan(0), (a) for predictions superimposed with the whole initial errors in the tropical Indian Ocean, (b–c) for predictions with targeted observation strategy conducted inside/outside the sensitive area in the tropical Indian Ocean, respectively.

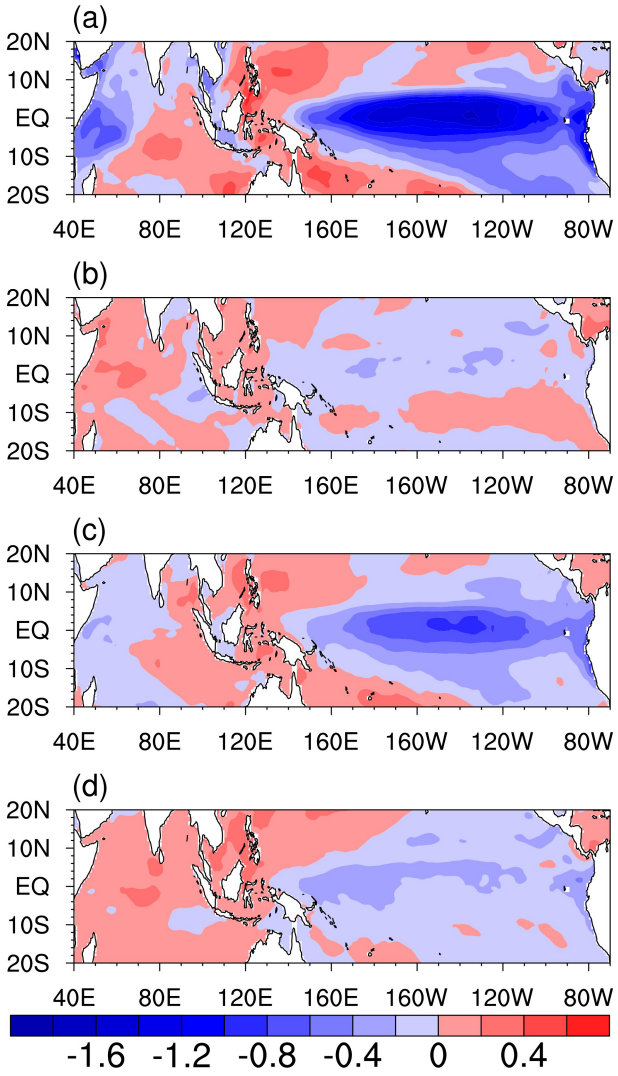

Fig. 10. Predicted SSTA in Dec(0) in the tropical oceans for La Niña predictions starting from Jan(0), (a) for the "true state" of La Niña events, (b) for predictions superimposed with the whole initial errors in the tropical Indian Ocean, (c–d) for the predictions with targeted observation strategy conducted inside/outside the sensitive area in the tropical Indian Ocean, respectively.

geted observation strategies are applied inside the sensitive area, positive prediction errors of sea temperature are still there, but both the magnitude and the area of the errors are reduced. As in Fig. 9c, when targeted observation strategies are adopted outside the sensitive area, the spatial pattern and the magnitude of the prediction errors are much like those from the control run, implying little improvements of La Niña prediction skill. The differences of prediction errors between these different sensitivity experiments support the former conclusion that adopting targeted observation strategies in the sensitive area in the Indian Ocean can significantly reduce the prediction errors and improve the forecast skill of La Niña events.

The predicted SSTA are also shown in Fig. 10. Figure 10a shows the "true state" of typical La Niña events, with negative SSTA prevailing in the tropical Pacific Ocean. When SPB-related initial errors exist in the tropical Indian Ocean, the La Niña event mode is disappeared due to the large influences from the IO-related initial errors. When targeted observation strategies are adopted outside the sensitive area in the Indian Ocean, as in Fig. 10d, predicted SSTA shows larger negative SSTA in the tropical Pacific Ocean when compared with that from Fig. 10b, showing some improvement. However, when targeted observation strategies are adopted inside the sensitive area in the tropical Indian Ocean (Fig. 10c,), the predicted SSTA in the tropical Pacific Ocean shows a typical La Niña mode pattern with a relatively reduced magnitude, implying that the prediction skill for La Niña events is significantly improved.

In short, La Niña prediction is sensitive to the sea temperature errors in the sensitive area which resides in the eastern tropical Indian Ocean, and it is very useful to apply targeted observations in this sensitive area, instead of other places, to obtain better La Niña forecasts.

7. Summary and discussion

The influences of IO-related sea temperature errors on La Niña predictions are explored by using coupled earth sys-

tem model CESM. From plenty of sensitivity experiments, the initial errors in the Indian Ocean that are most likely to yield the SPB for La Niña forecasts (i.e., SPB-related initial errors) are revealed. These SPB-related initial errors in the tropical Indian Ocean can be categorized into two types according to their spatial structures by cluster analysis. SPB-related Type-1 initial error has a positive IOD-like structure with positive errors of sea temperature in the western Indian Ocean and negative errors in the east. The structure of Type-2 initial error is nearly opposite to that of Type-1. For Type-1 initial error, which has a positive IOD-like error pattern in the tropical Indian Ocean, errors keep growing and persist in that spatial pattern by the end of the prediction; positive errors of sea temperature first show up in the central Pacific Ocean and develop into an El Niño-like error pattern by the end of the prediction. For Type-1 initial error, it is the atmospheric bridge that plays the crucial role in IO-related initial errors influencing the SSTA in the Pacific Ocean. For Type-2 initial error, which manifests in a negative IOD-like pattern, the prediction errors in the tropical Indian Ocean decay and then develop into a positive IOD-like pattern; meanwhile, the positive errors of sea temperature in the eastern Indian Ocean can lead to downwelling anomalies which can penetrate into the equatorial western Pacific Ocean through the ITF. Also for Type-2 initial error, the prediction errors of sea temperature in the tropical Pacific Ocean have an El Niño-like pattern at the end of the prediction. The sensitive area in the tropical Indian Ocean for La Niña forecasts is then identified based on those SPB-related initial errors. We also have evaluated the effectiveness of adopting targeted observation strategies in this sensitive area. The results indicate that the averaged benefit of applying targeted observations in the sensitive area is overwhelmingly large, even though the sensitive area is only one-fifth of the whole tropical Indian Ocean. So, it is much more effective to adopt targeted observation strategies inside the sensitive area rather than any other region.

Two types of optimal conditional initial errors in the tropical Indian Ocean that have the largest influences on La Niña predictions are explored in this study. Type-1 and Type-2 SPB-related initial errors, with positive and negative IOD-like structures respectively, are both very similar to the SPB-related initial errors in the tropical Indian Ocean of the El Niño predictions discovered by Zhou et al. (2019). Therefore, the Type-1 initial errors calculated from both the El Niño events and La Niña predictability studies are marked as "Type-1 initial error," and same for Type-2 initial errors. A brief summary is presented in Table 2. For El Niño forecasts, both Type-1 and Type-2 initial errors tend to have negative prediction errors of sea temperature in the tropical Pacific Ocean; the ITF and the atmospheric bridge play leading roles in IO-related Type-1 and Type-2 initial errors influencing the SSTA associated with ENSO prediction, respectively. When it comes to the La Niña forecasts, both types of IO-related initial errors tend to result in positive errors of sea temperature in the tropical Pacific Ocean, and IO-related Type-1 and Type-2 initial errors incline to influence the ENSO predictions by virtue of the atmospheric bridge and the ITF, respectively.

Even though these IO-related Type-1 and Type-2 initial errors for both El Niño and La Niña predictions have much in common, there are still some differences that cannot be neglected. For SPB-related Type-1 initial errors of El Niño, the positive errors dominate between 10°S and 10°N in the western Indian Ocean, while for Type-1 initial errors of La Niña, the positive errors only appear in the southern Western Indian Ocean. Ojha and Gnanaseelan (2015) suggest that a north-south dipole is the dominant mode in the subsurface. Unfortunately, the region for the initial errors in the tropical Indian Ocean is not big enough to include the whole southern pole in the subsurface in our study. More studies should be carried out if we want to figure out the similarity between the SPB-related Type-1 initial errors of La Niña and the subsurface dipole.

For the IO-related initial errors that have the largest influence on El Niño predictions with start month Jan(0), all the predictions tend to underestimate the magnitude of the La Niña events. This is also the case for most of the sensitivity experiments carried out during the study of La Niña predictions, with one exception represented by the purple line in Fig. 2b. Why is this initial error so special? Is it just a random case? Or may it have any implications? Two types of SPB-related initial errors are revealed in the tropical Indian Ocean, and the roles of both the ITF and the atmospheric bridge are analyzed. Are they independent? Can their influences be quantified? These questions will need to be answered in the future with more carefully designed sensitivity experiments and analyses.

In this study on La Niña predictability, we only use the traditional Niño-3 index to represent La Niña events. However, ENSO events are diverse, including both EP-type and CP-type (Kao and Yu, 2009; Kug et al., 2009) events, and prediction barriers exist for them both (Ren et al., 2016; Tian et al., 2019). So, more studies should be carried out to explore the different influences of IO-related initial errors on the two different types of ENSO events.

It can be concluded that both positive and negative IOD-like initial errors have the largest influences on the pre-

Table 2. A brief table of the influences of IO-related initial errors (both Type-1 and Type-2) on the SSTA predictions in the Pacific Ocean, and the possible main dynamical mechanisms behind them.

	Prediction errors induced by the IO-related initial errors	Dynamic mechanism for Type-1 initial errors	Dynamic mechanism for Type-2 initial errors
El Niño events	Negative initial errors	ITF	Atmospheric bridge
La Niña events	Positive initial errors	Atmospheric bridge	ITF

dictions of ENSO events, leading to the SPB phenomena. Mu and Jiang (2011) pointed out that the optimally growing initial errors in the onset predictions of blocking events and the optimal precursors that trigger the onsets have a lot in common. And the optimal precursors and the conditional nonlinear optimal perturbation always share similar structures (Mu et al.,, 2014, 2017). So, what is the optimal precursor of ENSO events in the tropical Indian Ocean? Will the optimal precursor in the tropical Indian Ocean share similar structures with these SPB-related initial errors? What's more, ensemble forecasts are one of the most useful ways to improve ENSO prediction skill, and a good ensemble forecast relies on good ensemble initial errors. So, could this kind of IO-related initial error that grows fastest be considered as one of the ensemble initial errors in order to improve the ensemble forecast skill? These questions can be explored in the future studies.

According to the large value area of these SPB-related initial errors, the sensitive area in the tropical Indian Ocean for La Niña forecasts is revealed. And adopting targeted observation strategies in this sensitive area can significantly decrease the prediction errors of La Niña forecasts. Zhou et al. (2020) have also identified the sensitive area in the Indian Ocean for El Niño forecasts. It can be noticed that, both kinds of sensitive areas mainly reside in the equatorial eastern Indian Ocean. So, whether this region can be treated as the common sensitive area for ENSO predictions is also one of our concerns. What's more, due to the large computational cost, sensitivity experiments of the targeted observations are only carried out with the SPB-related cases. Since most cases are not SPB-type, whether the sensitive area still works is another interesting question. So further studies should be carried out to answer these questions. Also because of the huge computational cost, only sensitivity experiments starting from Jan(0) are completed. More sensitivity experiments starting from other start months, such as Apr(0), Jul(0), and so on, should be completed to explore the influences of IO-related initial errors on SSTA forecasts during La Niña predictions bestriding its decaying phase.

The National Marine Environmental Forecast Center has an operational global SST forecast model, which also shows good performance for ENSO prediction (Zhang et al., 2018, 2019). Though the conclusions from this paper are all based on the "perfect model" assumption, it is still of our interests to apply them to operational forecasts to see how it works in real time. What are the influences of the initial errors of sea temperature in the tropical Indian Ocean on real La Niña predictions? Will the sensitive area identified in this study remain effective in operational forecast models? ENSO prediction skill can be further improved once these questions are answered with sensitivity experiments carried out with the operational forecast model.

In this study, we simply assume the model is perfect, so no model errors are considered. However, due to an overly strong Bjerknes feedback simulated in the equatorial Indian Ocean, most Coupled Model Intercomparison Project Phase Three (CMIP3) and CMIP5 models (including the CESM we used in this study) have IOD bias (Cai and Cowan, 2013). Moreover, like many other coupled models, the CESM also has an overly strong variability of sea surface temperature in the eastern Indian Ocean because of its exaggerated sensitivity to thermocline variations (Wieners et al., 2019). Our conclusions may be model-dependent since we only use the CESM, which is also flawed, to complete the sensitivity experiments. If we can reduce the model errors in ENSO predictions following the strategy of Tao et al. (2020) (i.e., using the Nonlinear Forcing Singular Vector (NFSV) approach), ENSO prediction skill may be further improved.

Acknowledgements. This study was supported by the National Key R&D Program of China (Grant No. 2019YFC1408004), together with the National Natural Science Foundation of China (Grant Nos. 41930971, 41805069, 41606031) and the Office of China Postdoctoral Council (OCPC) under Award Number 20190003

REFERENCES

Barber, R. T., and F. P. Chavez, 1983: Biological consequences of El Niño. *Science*, **222**, 1203–1210, https://doi.org/10.1126/science.222.4629.1203.

Behera, S. K., and T. Yamagata, 2003: Influence of the Indian Ocean dipole on the Southern Oscillation. *J. Meteor. Soc. Japan*, **81**, 169–177, https://doi.org/10.2151/jmsj.81.169.

Bunge, L., and A. J. Clarke, 2014: On the warm water volume and its changing relationship with ENSO. *J. Phys. Oceanogr.*, **44**, 1372–1385, https://doi.org/10.1175/JPO-D-13-062.1.

Cai, W. J., and T. Cowan, 2013: Why is the amplitude of the Indian Ocean dipole overly large in CMIP3 and CMIP5 climate models? *Geophys. Res. Lett.*, **40**, 1200–1205, https://doi.org/10.1002/grl.50208.

Cortés, G., and S. Margulis, 2017: Impacts of El Niño and La Niña on interannual snow accumulation in the Andes: Results from a high-resolution 31 year reanalysis. *Geophys. Res. Lett.*, **44**, 6859–6867, https://doi.org/10.1002/2017GL073826.

Ding, S. Y., W. Chen, J. Feng, and H. F. Graf, 2017: Combined impacts of PDO and two types of La Niña on climate anomalies in Europe. *J. Climate*, **30**, 3253–3278, https://doi.org/10.1175/JCLI-D-16-0376.1.

Duan, W. S., and J. Y. Hu, 2016: The initial errors that induce a significant "spring predictability barrier" for El Niño events and their implications for target observation: Results from an earth system model. *Climate Dyn.*, **46**, 3599–3615, https://doi.org/10.1007/s00382-015-2789-5.

Feng, R., W. S. Duan, and M. Mu, 2014: The "winter predictability barrier" for IOD events and its error growth dynamics: Results from a fully coupled GCM. *J. Geophys. Res.: Oceans*, **119**, 8688–8708, https://doi.org/10.1002/2014JC010473.

Gao, C., X. R. Wu, and R. H. Zhang, 2016: Testing a four-dimensional variational data assimilation method using an improved intermediate coupled model for ENSO analysis and prediction. *Adv. Atmos. Sci.*, **33**, 875–888, https://doi.org/10.1007/s00376-016-5249-1.

Gao, H., and S. Yang, 2009: A severe drought event in northern China in winter 2008–2009 and the possible influences of La Niña and Tibetan Plateau. *J. Geophys. Res.: Atmos.*, **114**, D24104, https://doi.org/10.1029/2009JD012430.

Gordon, A. L., 2005: Oceanography of the indonesian seas and their throughflow. *Oceanography*, **18**, 14–27, https://doi.org/10.5670/oceanog.2005.01.

Ham, Y. G., M. K. Sung, S. I. An, S. D. Schubert, and J. S. Kug, 2014: Role of tropical atlantic SST variability as a modulator of El Nio teleconnections. *Asia-Pacific Journal of Atmospheric Sciences*, **50**, 247–261, https://doi.org/10.1007/s13143-014-0013-x.

Henderson, D. S., C. D. Kummerow, and W. Berg, 2018: ENSO influence on TRMM tropical oceanic precipitation characteristics and rain rates. *J. Climate*, **31**, 3979–3998, https://doi.org/10.1175/JCLI-D-17-0276.1.

Hermes, J. C., and Coauthors, 2019: A sustained ocean observing system in the Indian Ocean for climate related scientific knowledge and societal needs. *Frontiers in Marine Science*, **6**, 355, https://doi.org/10.3389/fmars.2019.00355.

Huang, R. H., W. Chen, B. L. Yang, and R. H. Zhang, 2004: Recent advances in studies of the interaction between the East Asian winter and summer monsoons and ENSO cycle. *Adv. Atmos. Sci.*, **21**, 407–424, https://doi.org/10.1007/BF02915568.

Hurrell, J. W., and Coauthors, 2013: The community earth system model: A framework for collaborative research. *Bull. Amer. Meteor. Soc.*, **94**, 1339–1360, https://doi.org/10.1175/BAMS-D-12-00121.1.

Izumo, T., M. Lengaigne, J. Vialard, J. J. Luo, T. Yamagata, and G. Madec, 2014: Influence of Indian Ocean dipole and Pacific recharge on following year's El Niño: Interdecadal robustness. *Climate Dyn.*, **42**, 291–310, https://doi.org/10.1007/s00382-012-1628-1.

Izumo, T., and Coauthors, 2010: Influence of the state of the Indian Ocean dipole on the following year's El Niño. *Nature Geoscience*, **3**, 168–172, https://doi.org/10.1038/ngeo760.

Kao, H. Y., and J. Y. Yu, 2009: Contrasting Eastern-Pacific and Central-Pacific types of ENSO. *J. Climate*, **22**, 615–632, https://doi.org/10.1175/2008JCLI2309.1.

Kirtman, B., J. Shukla, M. Balmaseda, N. Graham, C. Penland, Y. Xue, and S. Zebiak, 2001: Current Status of ENSO Forecast Skill. WCRP Informal Report No 23/01.

Kug, J. S., F. F. Jin, and S. I. An, 2009: Two types of El Niño events: Cold tongue El Niño and warm pool El Niño. *J. Climate*, **22**, 1499–1515, https://doi.org/10.1175/2008JCLI2624.1.

Lim, E. P., and H. H. Hendon, 2017: Causes and predictability of the negative Indian Ocean dipole and its impact on La Niña during 2016. *Scientific Reports*, **7**, 12619, https://doi.org/10.1038/s41598-017-12674-z.

Lopez, H., and B. P. Kirtman, 2014: WWBs, ENSO predictability, the spring barrier and extreme events. *J. Geophys. Res.: Atmos.*, **119**, 10 114–10 138, https://doi.org/10.1002/2014JD021908.

Lu, F. Y., Z. Y. Liu, Y. Liu, S. Q. Zhang, and R. Jacob, 2017: Understanding the control of extratropical atmospheric variability on ENSO using a coupled data assimilation approach. *Climate Dyn.*, **48**, 3139–3160, https://doi.org/10.1007/s00382-016-3256-7.

Luo, J. J., R. C. Zhang, S. K. Behera, Y. Masumoto, F. F. Jin, R. Lukas, and T. Yamagata, 2010: Interaction between El Niño and extreme Indian Ocean dipole. *J. Climate*, **23**, 726–742, https://doi.org/10.1175/2009JCLI3104.1.

Matei, D., N. Keenlyside, M. Latif, and J. Jungclaus, 2008: Subtropical forcing of tropical Pacific climate and decadal ENSO modulation. *J. Climate*, **21**, 4691–4709, https://doi.org/10.1175/2008JCLI2075.1.

McPhaden, M. J., 2003: Tropical Pacific Ocean heat content variations and ENSO persistence barriers. *Geophys. Res. Lett.*, **30**, 1480, https://doi.org/10.1029/2003GL016872.

Meng, W., and G. X. Wu, 2000: Gearing between the Indo-Monsoon Circulation and the Pacific-Walker circulation and the ENSO Part II: Numerical simulation. *Chinese Journal of Atmospheric Sciences*, **24**, 15–25. (in Chinese with English abstract)

Moore, A. M., and Coauthors, 2006: Optimal forcing patterns for coupled models of ENSO. *J. Climate*, **19**, 4683–4699, https://doi.org/10.1175/JCLI3870.1.

Mu, M., 2013: Methods, current status, and prospect of targeted observation. *Science China Earth Sciences*, **56**, 1997–2005, https://doi.org/10.1007/s11430-013-4727-x.

Mu, M., and Z. N. Jiang, 2011: Similarities between optimal precursors that trigger the onset of blocking events and optimally growing initial errors in onset prediction. *J. Atmos. Sci.*, **68**, 2860–2877, https://doi.org/10.1175/JAS-D-11-037.1.

Mu, M., Q. Wang, W. S. Duan, and Z. N. Jiang, 2014: Application of conditional nonlinear optimal perturbation to targeted observation studies of the atmosphere and ocean. *J. Meteor. Res.*, **28**, 923–933, https://doi.org/10.1007/s13351-014-4057-8.

Mu, M., W. S. Duan, D. K. Chen, and W. D. Yu, 2015: Target observations for improving initialization of high-impact ocean-atmospheric environmental events forecasting. *National Science Review*, **2**, 226–236, https://doi.org/10.1093/nsr/nwv021.

Mu, M., R. Feng, and W. S. Duan, 2017: Relationship between optimal precursors for Indian Ocean dipole events and optimally growing initial errors in its prediction. *J. Geophys. Res.: Oceans*, **122**, 1141–1153, https://doi.org/10.1002/2016JC012527.

Ojha, S., and C. Gnanaseelan, 2015: Tropical Indian Ocean subsurface temperature variability and the forcing mechanisms. *Climate Dyn.*, **44**, 2447–2462, https://doi.org/10.1007/s00382-014-2379-y.

Ren, H. L., F. F. Jin, B. Tian, and A. A. Scaife, 2016: Distinct persistence barriers in two types of ENSO. *Geophys. Res. Lett.*, **43**, 10 973–10 979, https://doi.org/10.1002/2016GL071015.

Rodríguez-Fonseca, B., I. Polo, J. García-Serrano, T. Losada, E. Mohino, C. R. Mechoso, and F. Kucharski, 2009: Are Atlantic Niños enhancing Pacific ENSO events in recent decades? *Geophys. Res. Lett.*, **36**, L20705, https://doi.org/10.1029/2009GL040048.

Snyder, C., 1996: Summary of an informal workshop on adaptive observations and FASTEX. *Bull. Amer. Meteor. Soc.*, **77**, 953–961, https://doi.org/10.1175/1520-0477-77.5.953.

Tao, L. J., W. S. Duan, and S. Vannitsem, 2020: Improving forecasts of El Niño diversity: A nonlinear forcing singular vector approach. *Climate Dyn.*, **55**, 739–754, https://doi.org/10.1007/s00382-020-05292-5.

Tian, B., H. L. Ren, F. F. Jin, and M. F. Stuecker, 2019: Diagnosing the representation and causes of the ENSO persistence barrier in CMIP5 simulations. *Climate Dyn.*, **53**, 2147–2160, https://doi.org/10.1007/s00382-019-04810-4.

Tillinger, D., and A. L. Gordon, 2009: Fifty years of the indonesian throughflow. *J. Climate*, **22**, 6342–6355, https://doi.org/10.1175/2009JCLI2981.1.

Wang, B., R. G. Wu, and X. H. Fu, 2000: Pacific-East Asian teleconnection: How does ENSO affect East Asian climate? *J. Climate*, **13**, 1517–1536, https://doi.org/10.1175/1520-0442(2000)013<1517:PEATHD>2.0.CO;2.

Wang, X., D. X. Wang, W. Zhou, and C. Y. Li, 2012: Interdecadal modulation of the influence of La Niña events on mei-yu rainfall over the Yangtze River valley. *Adv. Atmos. Sci.*, **29**, 157–168, https://doi.org/10.1007/s00376-011-1021-8.

Wieners, C. E., H. A. Dijkstra, and W. P. M. de Ruijter, 2019: The interaction between the Western Indian Ocean and ENSO in CESM. *Climate Dyn.*, **52**, 5153–5172, https://doi.org/10.1007/s00382-018-4438-2.

Wu, G. X., and W. Meng, 1998: Gearing between the indo-monsoon circulation and the pacific-walker circulation and the ENSO. Part 1. Data analyses. *Scientia Atmospherica Sinica*, **22**, 470–480. (in Chinese with English abstract)

Wu, R. G., M. Y. Lin, and H. M. Sun, 2020: Impacts of different types of El Niño and La Niña on northern tropical Atlantic sea surface temperature. *Climate Dyn.*, **54**, 4147–4167, https://doi.org/10.1007/s00382-020-05220-7.

Xu, T. F., D. L. Yuan, Y. Q. Yu, and X. Zhao, 2013: An assessment of Indo-Pacific Oceanic channel dynamics in the FGOALS-g2 coupled climate system model. *Adv. Atmos. Sci.*, **30**, 997–1016, https://doi.org/10.1007/s00376-013-2131-2.

Xue, F., Q. C. Zeng, R. H. Huang, C. Y. Li, R. Y. Lu, and T. J. Zhou, 2015: Recent advances in monsoon studies in China. *Adv. Atmos. Sci.*, **32**, 206–229, https://doi.org/10.1007/s00376-014-0015-8.

Yang, S., Z. N. Li, J. Y. Yu, X. M. Hu, W. J. Dong, and S. He, 2018: El Niño-Southern Oscillation and its impact in the changing climate. *National Science Review*, **5**, 840–857, https://doi.org/10.1093/nsr/nwy046.

Yu, J. Y., C. R. Mechoso, J. C. McWilliams, and A. Arakawa, 2002: Impacts of the Indian Ocean on the ENSO cycle. *Geophys. Res. Lett.*, **29**, 46-1–46-4, https://doi.org/10.1029/2001GL014098.

Yuan, D., and Coauthors, 2011: Forcing of the Indian Ocean dipole on the interannual variations of the tropical Pacific Ocean: Roles of the indonesian throughflow. *J. Climate*, **24**, 3593–3608, https://doi.org/10.1175/2011JCLI3649.1.

Yuan, D. L., H. Zhou, and X. Zhao, 2013: Interannual climate variability over the tropical Pacific Ocean induced by the Indian Ocean dipole through the indonesian throughflow. *J. Climate*, **26**, 2845–2861, https://doi.org/10.1175/JCLI-D-12-00117.1.

Zhang, R. H., and S. E. Zebiak, 2002: Effect of penetrating momentum flux over the surface boundary/mixed layer in a z-Coordinate OGCM of the tropical Pacific. *J. Phys. Oceanogr.*, **32**, 3616–3637, https://doi.org/10.1175/1520-0485(2002)032<3616:EOPMFO>2.0.CO;2.

Zhang, R. H., and Coauthors, 2020a: A review of progress in coupled ocean-atmosphere model developments for ENSO studies in China. *Journal of Oceanology and Limnology*, **38**, 930–961, https://doi.org/10.1007/s00343-020-0157-8.

Zhang, S. W., C. Y. Song, H. Wang, H. Jiang, and L. Du, 2018: Evaluation of the hindcasting main SSTA modes of the global key regions based on the CESM forecasting system. *Haiyang Xuebao*, **40**, 18–30, https://doi.org/10.3969/j.issn.0253-4193.2018.09.002. (in Chinese with English abstract)

Zhang, S. W., H. Jiang, and H. Wang, 2019: Assessment of the sea surface temperature predictability based on multimodel hindcasts. *Wea. Forecasting*, **34**, 1965–1977, https://doi.org/10.1175/WAF-D-19-0040.1.

Zhang, S. Q., and Coauthors, 2020b: Coupled data assimilation and parameter estimation in coupled ocean-atmosphere models: A review. *Climate Dyn.*, **54**, 5127–5144, https://doi.org/10.1007/s00382-020-05275-6.

Zhou, Q., W. S. Duan, M. Mu, and R. Feng, 2015: Influence of positive and negative Indian Ocean dipoles on ENSO via the indonesian throughflow: Results from sensitivity experiments. *Adv. Atmos. Sci.*, **32**, 783–793, https://doi.org/10.1007/s00376-014-4141-0.

Zhou, Q., M. Mu, and W. S. Duan, 2019: The initial condition errors occurring in the Indian Ocean temperature that cause "Spring Predictability Barrier" for El Niño in the Pacific Ocean. *J. Geophys. Res.: Oceans*, **124**, 1244–1261, https://doi.org/10.1029/2018JC014403.

Zhou, Q., W. S. Duan, and J. Y. Hu, 2020: Exploring sensitive area in the tropical Indian Ocean for El Niño prediction: Implication for targeted observation. *Journal of Oceanology and Limnology*, **38**, 1602–1615, https://doi.org/10.1007/s00343-019-9062-4.

Zhu, J. S., B. H. Huang, M. A. Balmaseda, J. L. Kinter, P. T. Peng, Z. Z. Hu, and L. Marx, 2013: Improved reliability of ENSO hindcasts with multi-ocean analyses ensemble initialization. *Climate Dyn.*, **41**, 2785–2795, https://doi.org/10.1007/s00382-013-1965-8.

Zhu, Y. C., R. H. Zhang, and J. C. Sun, 2020: North Pacific upper-ocean cold temperature biases in CMIP6 simulations and the role of regional vertical mixing. *J. Climate*, **33**, 7523–7538, https://doi.org/10.1175/JCLI-D-19-0654.1.